Journal of
Ceramic Science
and Technology

J. Ceram. Sci. Technol., **08** [3] 351-364 (2017)
DOI: 10.4416/JCST2017-00035
available online at: http://www.ceramic-science.com

Intumescent Geopolymer-Bound Coatings for Fire Protection of Steel

M.-B. Watolla[1], G.J.G. Gluth[*1], P. Sturm[1], W.D.A. Rickard[2], S. Krüger[1], B. Schartel[1]

[1]Bundesanstalt für Materialforschung und -prüfung (BAM), Unter den Eichen 87, D-12205 Berlin, Germany
[2]Curtin University, John de Laeter Centre and Department of Physics & Astronomy, GPO Box U1987, Perth WA 6845, Australia

received May 19, 2017; received in revised form August 10, 2017; accepted August 24, 2017

Abstract

The passive fire protection of steel structures and other load-bearing components will continue to gain importance in future years. In the present contribution, novel intumescent aluminosilicate (geopolymer-bound) composites are proposed as fire-protective coatings on steel. Steel plates coated with these materials were exposed to the standard temperature-time curve as defined in ISO 834 – 1:1999. The coatings partially foamed during curing and expanded further during thermal exposure, demonstrating their intumescent characteristic. Thermogravimetry and oscillatory rheometry determined that the intumescent behavior is attributed to a transition to a viscous state (loss factor > 1) in the temperature range of major water release, differing from conventional geopolymers. XRD and SEM images showed that the coatings had characteristics of ceramic or glass-ceramic foams after fire resistance testing, suggesting superior performance under challenging conditions. The thickness of the coatings influenced their foaming and intumescent behavior and thus the time for the coated steel plates to reach 500 °C. A number of additives were also studied with the best performance obtained from samples containing sodium tetraborate. A coating of just 6 mm was able to delay the time it takes for a steel substrate to reach 500 °C to more than 30 minutes.

Keywords: Geopolymers, aluminosilicate inorganic polymers, intumescence, coatings, fire resistance, fire protection

I. Introduction

Passive fire-protective coatings for structural components, e.g. made from steel or wood, can be grouped into two classes: thin, reactive intumescent coatings and thick, non-reactive fire protection coatings such as blankets, sprays, and ablative or insulating coatings. While, in general, both classes of coatings are able to fulfill the requirements to provide sufficient fire protection, intumescent coatings can possess advantages regarding aesthetics, weight per unit area, speed of construction, quality control and also cost efficiency. This has led to increased scientific and commercial interest in this type of coatings in recent decades [1–7], and several reviews on this topic have been published recently [8–10].

The vast majority of intumescent coatings described in the literature are based on the 'classic' system of acid source + char former + blowing agent + binder (organic polymer), or variants of it [1,8,9]; thus, they contain a significant fraction of organic compounds, and the foam that forms during intumescence contains essentially carbonaceous char. More recent approaches include silicon-based coatings containing expandable graphite and/or organoclay particles [11–13] as well as coatings containing significant amounts of 'ceramic precursors' [14,15]. These systems have the advantage of producing a mechanically and thermally more stable residue after foaming, which can make them suitable for more aggressive environments, e.g. higher temperatures, longer duration, and/or environments with a higher concentration of abrasive particles or corroding gases. Owing to increased demands of society and industry, this field of research – i.e. fire-protective coatings for extreme conditions – will continue to grow and will lead to the development of new materials and test methods [16].

Geopolymers are a class of inorganic binders/cements that are based on the alkaline activation of solid aluminosilicate feedstocks, and which differ in many respects from conventional cements [17,18]. In particular, geopolymers and geopolymeric materials can possess significantly better resistance against high temperatures than conventional Portland-cement-based materials. Depending on their composition, geopolymers retain their amorphous structure or form ceramic phases without significant decomposition on heating to temperatures that occur in refractory applications or in a fire [19–25]. This makes them promising candidates as refractory materials [20,26], as binders for the production of concretes with high-temperature resistance [27–29] as well as for the production of fire-protective coatings [30–35] and related materials [36]. In the context of coating applications, foaming of geopolymer pastes in the fresh state and the properties of foamed geopolymers have been the subject of significant attention [30,33,34,37–39].

In contrast, only few studies report about foaming/expansion of hardened geopolymers, i.e. intumescence of geopolymers. Lyon *et al.* [36] reported an approx. 500 %

* Corresponding author: gregor.gluth@bam.de

volume expansion of a geopolymer resin with very high SiO_2/Al_2O_3 molar ratio, but did not give the temperature of expansion onset. In a more recent study [40], foaming of geopolymers with high fractions of SiO_2, Na_2O and H_2O was observed when heated to above approx. 100 – 225 °C, the actual temperature of foaming onset depending on the amount of these components relative to Al_2O_3. Qualitatively equivalent results have been reported by others [23, 41], but much lower expansion was observed in these latter studies. The study by Krivenko *et al.* [31] contains more detailed results on the influence of aluminosilicate composition as well as of additives and the mode of application on the volume increase when heated, and the authors suggest applying the intumescent materials described in their study as fire-protective coatings for metal, concrete, brickwork and wood.

In the present contribution, a novel intumescent aluminosilicate formulation developed at Curtin University is compared with a formulation adopted from the latter study [31]. Microstructural characterization before and after fire resistance tests was done by means of X-ray diffraction (XRD) and scanning electron microscopy (SEM). Thermogravimetric analyses (TGA) and oscillatory rheology measurements were conducted to examine the processes underlying the intumescent behavior. In the second part of the study, steel plates were coated with the two formulations and subjected to the standard temperature-time curve according to ISO 834 – 1:1999. The influence of additives (aluminum hydroxide, magnesium hydroxide, boron trioxide and sodium tetraborate) on the performance of the coatings is also reported and discussed.

II. Experimental

(1) Starting materials

Starting materials were microsilica, metakaolin, alumina, two sodium silicate solutions ('waterglass A' and 'waterglass B') and sodium hydroxide solution. Waterglass A had a composition of 29.8 ± 0.8 wt% SiO_2, 14.8 ± 0.8 wt% Na_2O, residual: H_2O (manufacturer's data). Waterglass B was produced by dissolving sodium hydroxide pellets and fumed silica (Aerosil 200) in water in proportions to yield a composition of 32.0 wt% SiO_2, 16.6 wt% Na_2O, 51.3 wt% H_2O, and stirring overnight. The sodium hydroxide solution was produced from NaOH pellets and deionized water and had a composition of 27.7 wt% Na_2O, 72.3 wt% H_2O. The chemical composition of the other feedstocks was determined using inductively coupled plasma optical emission spectrometry (ICP-OES) after total digestion. Powder X-ray diffraction (XRD; see Section II (3) for measurement conditions) was used to determine the phase assemblage of the feedstocks. The results are shown in Table 1 and in Fig. 1.

The diffractogram of the microsilica exhibits an amorphous hump centered at 21.3° 2θ and minor reflections from the impurities silicon (PDF # 00 – 001 – 0787) and silicon carbide (PDF # 00 – 049 – 1429). The metakaolin [KM 60; Keramost, Most, Czech Republic] contained crystalline impurities kaolinite (PDF # 00 – 014 – 0164), muscovite (PDF # 00 – 007 – 0025), illite (PDF 00 – 026 – 0911) and quartz (PDF # 00 – 046 – 1045), which are common minerals in kaolinite-bearing rocks. The specific surface area of the metakaolin was measured by means of nitrogen adsorption at 77 K, using the BET method for data evaluation, to be 9.9 m^2/g. The alumina consisted mainly of α-Al_2O_3 (corundum; PDF # 00 – 046 – 1212), but in addition contained a small amount of the low-sodium aluminate phase diaoyudaoite ($NaAl_{11}O_{17}$; PDF # 01 – 079 – 2288).

Table 1: Chemical composition of the solid starting materials (in wt%).

Component	Microsilica	Metakaolin	Alumina
SiO_2	95.16	50.62	< 0.01
Al_2O_3	0.17	42.31	99.03
Fe_2O_3	0.04	1.08	0.03
TiO_2	< 0.01	0.51	< 0.01
CaO	1.71	0.12	0.43
MgO	0.28	0.06	0.02
Na_2O	0.19	0.11	0.14
K_2O	0.65	0.88	0.03
SO_3	0.25	0.15	0.07
LOI	1.12	3.40	
Residual	0.45	0.80	0.15

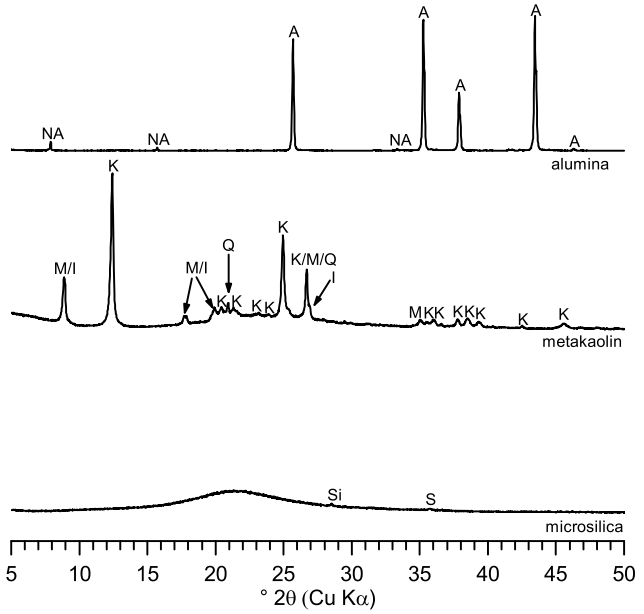

Fig. 1: Diffractograms of the solid starting materials (A = corundum; NA = diaoyudaoite; M = muscovite; I = illite; K = kaolinite; Q = quartz; Si = silicon; S = silicon carbide).

Additives for modification of the coatings were aluminum hydroxide ($Al(OH)_3$), magnesium hydroxide ($Mg(OH)_2$), boron trioxide (B_2O_3) and sodium tetraborate ($Na_2B_4O_7$; 'anhydrous borax'). All materials were commercially available compounds. The boron trioxide and the sodium tetraborate were ground in a ball mill for approx. 5 min before use. XRD (see Section II (3) for measurement conditions; results not displayed) showed the

sodium tetraborate to be amorphous with minor amounts of crystalline sodium tetraborate pentahydrate ($Na_2B_4O_7 \cdot 5H_2O$) present as an impurity; some very minor reflections of crystalline $Na_2B_4O_7$ were also present in the diffractogram. The other additives were used without any further processing.

(2) Materials

Two aluminosilicate formulations were studied regarding their applicability as fire-protective coatings; a conventional geopolymer was tested only with TGA and oscillatory rheometry for comparison purposes:

a) C1 was developed at Curtin University. Starting materials for C1 were microsilica, alumina and sodium hydroxide solution. The starting materials were mixed in proportions to yield a total stoichiometry of approx. $0.5Na_2O \cdot Al_2O_3 \cdot 2.4SiO_2 \cdot 4.9H_2O$; the design of C1 is given in Table 2.
b) K1b was adopted from Krivenko *et al.* [31], except that the water content of the mixture was reduced, because significant sedimentation before hardening was observed for pastes with the original composition. Starting materials for K1b were metakaolin, microsilica and waterglass A. The starting materials were mixed in proportions to yield a total stoichiometry of approx. $Na_2O \cdot Al_2O_3 \cdot 6.5SiO_2 \cdot 13.6H_2O$; the design of K1b is given in Table 2.
c) MK-ref was produced from metakaolin and waterglass B in proportions to yield a total stoichiometry of $Na_2O \cdot Al_2O_3 \cdot 4.0SiO_2 \cdot 11.0H_2O$; the design of MK-ref is given in Table 2. This non-intumescing geopolymer was produced for comparison purposes, as metakaolin-based geopolymers of this composition or close to it have been found to exhibit optimal mechanical properties and have been extensively studied [42–45].

The mass fractions and molar ratios of Na_2O, Al_2O_3, SiO_2 and H_2O of the formulations are summarized in Table 3. It is noted that the total molar ratios (i.e. the total stoichiometry) of the starting mixtures do not necessarily correspond to the actual composition of the geopolymeric gel, as the solid feedstocks dissolve and react only partially.

Production of the pastes was conducted as follows: The solid starting materials were mixed manually in a beaker; subsequently, the liquid component ('activator') was added. The beaker was sealed and placed in a contact-free planetary centrifugal mixer (Thinky), and the paste mixed for 4.5 min at 1600 rpm.

In addition to the aluminosilicate coatings as described above, pastes/coatings containing additives (see Section II (1)) were produced to study the influence of the additives on the performance in fire testing. All additives were added to the beaker together with the other solid precursors, i.e. before addition of the activator; subsequent mixing was done as for the aluminosilicate coatings. The amounts of additives are quoted as fractions relative to the total mass of the coating; the relative proportions of the other precursors were kept as in the coatings without additives in all cases. For example, a batch of the K1b coating with 10 wt% $Mg(OH)_2$ contained 26.60 wt% metakaolin, 16.62 wt% microsilica, 10.00 wt% $Mg(OH)_2$ and 46.77 wt% waterglass A. Coatings with different amounts of additives were studied; these amounts are given below where the pertinent results are reported (Section IV (2)).

After mixing, the pastes were poured onto stainless steel plates (75 mm × 75 mm × 2 mm; steel grade 1.4301, cleaned by means of sand blasting and rinsing with ethanol) which were placed in silicone molds (80 mm × 80 mm × 7 mm or 20 mm). With this set-up, coatings with defined heights between 3 and 12 mm were produced. As the molds had slightly larger lateral dimensions than the steel plates, the edges of the steel plate were coated, which minimized heat transfer to the steel plates *via* the edges during the fire tests. In parallel to the production of the coatings, small cubes (20 mm × 20 mm × 20 mm; for TGA and XRD measurements) and prismatic specimens (approx. 5 mm × 10 mm × 60 mm; for oscillatory rheometry measurements) were produced using silicone molds.

Table 2: Mix-design of the coatings.

	Metakaolin (wt%)	Microsilica (wt%)	Alumina (wt%)	NaOH sln. (wt%)	Waterglass A (wt%)	Waterglass B (wt%)
C1	-	40.90	27.20	31.90	-	-
K1b	29.56	18.47	-	-	51.97	-
MK-ref	39.44	-	-	-	-	60.56

Table 3: Fractions and total molar ratios of the main oxides of the coatings.

	$m(Na_2O)$ (wt%)	$m(Al_2O_3)$ (wt%)	$m(SiO_2)$ (wt%)	$m(H_2O)$ (wt%)	Na_2O/Al_2O_3 (mol/mol)	SiO_2/Al_2O_3 (mol/mol)	H_2O/Al_2O_3 (mol/mol)
C1	8.91	27.13	38.92	23.66	0.54	2.43	4.94
K1b	7.75	12.54	48.00	30.40	1.02	6.50	13.56
MK-ref	10.11	16.69	39.33	32.42	1.00	4.00	11.00

All samples were cured in a heating cabinet at 40 °C for 24 h; a humid atmosphere was maintained during curing by placing the samples in a sealed box together with an open beaker filled with water to prevent the materials from drying out. After curing, the samples were removed from the silicone molds and subsequently stored between one and three weeks at 23 °C and 50 % RH in a climate chamber before testing. Before fire testing, two thermocouples (type K) were spot-welded onto the back side of each coated steel plate, approximately in the center of the plates.

(3) Analytical methods

Samples for X-ray diffraction (XRD) and thermogravimetric analysis (TGA) were obtained from cured cubes and from coated steel plates after fire testing. Grinding was done manually with mortar and pestle (agate). The ground powders were stored in a desiccator over dried silica gel at ambient temperature until analysis.

XRD measurements were performed on an Ultima IV device supplied by Rigaku under the following experimental conditions: Bragg-Brentano geometry; CuKα radiation (λ = 1.5419 Å); scanning range: 5 – 65° 2θ; scanning speed: 0.5° 2θ/min; step width: 0.02° 2θ; sample rotation speed: 15 rpm. Sample holders were filled using the front-loading procedure.

TGA was performed with a TG 209 F1 Iris supplied by Netzsch (Selb, Germany). 5 mg of material was heated from 30 °C to 900 °C at a heating rate of 10 K/min under flowing nitrogen (20 ml/min). Two samples were measured for each material and the results averaged.

Oscillatory rheological measurements were conducted with a MCR 501 rheometer by Anton Paar (Ostfilder-Scharnhausen, Germany). Rod-like shaped samples (approx. 5 mm × 10 mm × 60 mm; length between clamping points 25 mm) were tested at a constant frequency of 1 Hz with a deformation amplitude of 0.05 %. A heating rate of 10 K/min was applied to heat up the samples during the measurements from room temperature to 300 °C.

The microstructure of the intumescent coatings was investigated using a Tescan LYRA3 scanning electron microscope (SEM). Cross-sectional fracture surfaces were sampled from coatings in a representative region near the center of the steel plates. Micrographs were captured using an acceleration voltage of 20 kV and either a secondary electron (SE) or a backscattered electron (BSE) detector.

(4) Fire resistance testing

The fire resistance of the samples was investigated in a furnace with an internal volume of approx. 1 m^3. Vermiculite plates with nine square cavities, each with a small hole for the connection of the thermocouples on the backside, were used to hold the samples. The specimens were installed in the cavities so as to expose the coating to the furnace, and the thermocouples at the back side of each plate connected to a data logger. A detailed description of the set-up has been given elsewhere [16].

The temperature inside the furnace was continuously controlled with two oil burners and recorded using thermocouples to adjust the power of the oil burners when necessary. The excess pressure inside the furnace was kept at 10 Pa during all tests. The temperature in the furnace followed the standard temperature-time curve specified as the heating curve in ISO 834 – 1:1999. Depending on the performance of the coatings, most measurements were stopped after 30 min, by turning off the oil burners, and the furnace and the samples allowed to cool down naturally to room temperature. During all tests, the temperatures at the back side of the coated steel plates and at least one uncoated steel plate (for comparison) were recorded.

III. Properties of the Aluminosilicate Coatings

(1) Phase assemblage before and after fire resistance testing

The results of the XRD investigations on the cured C1 and the fire residue of C1 are shown in Fig. 2. The results from the as-cured sample indicate only amorphous reaction products. The maximum of the microsilica at 21.3° 2θ diminished and a new maximum occurred at 25.8° 2θ; this indicates a mixture of unreacted microsilica and X-ray amorphous geopolymeric gel, which generally causes a broad hump centered at around 27 – 29° 2θ [46]. Significant amounts of alumina, including the diaoyudaoite, remained in the cured system, evidencing the expected incomplete reaction of this feedstock.

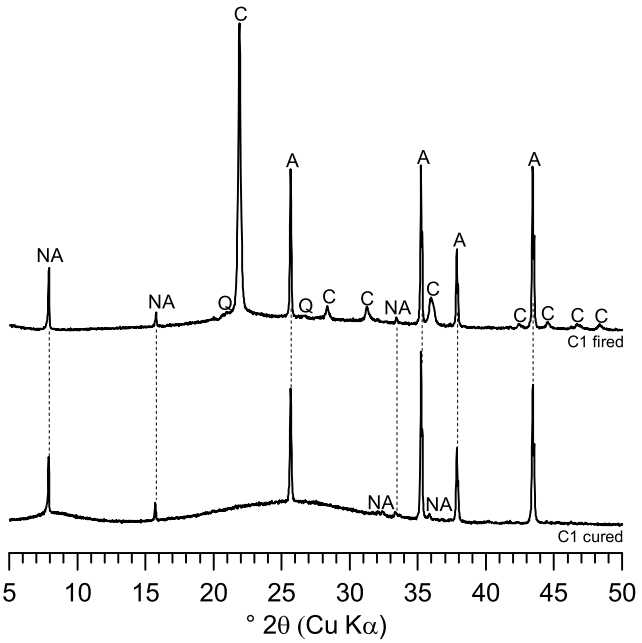

Fig. 2: Diffractograms of C1 and its fire residue (A = corundum; NA = diaoyudaoite; Q = quartz; C = cristobalite).

After fire resistance testing (max. temperature approx. 840 °C) of C1 the unreacted alumina remained largely unaffected, although slight changes of the relative peak heights of the corundum were observed in the diffractogram. The maximum of the hump in the diffractogram shifted to lower angles (maximum at approx. 22° 2θ), indicating that the geopolymeric gel was destroyed or at least altered significantly. Major reflections of cristobalite (PDF # 01 – 076 – 0941) and minor reflections of quartz, most likely produced by transformation of the microsilica, are present in the diffractogram. It is noted that conversion of silica to cristobalite is normally expected at temperatures above 1000 – 1200 °C [47]; however, it has been observed

that this conversion takes place at significantly lower temperatures in the presence of alkali silicates [48,49].

As for C1, XRD indicated an incomplete reaction of the solid feedstocks for K1b (Fig. 3). All crystalline impurities from the metakaolin (muscovite, illite, kaolinite, quartz) were observed after curing. A hump with a maximum at around 27° 2θ indicates the formation of geopolymeric gel. Very minor amounts of zeolite Na-A (framework type LTA; PDF # 00–039–0222) were present in the material after curing.

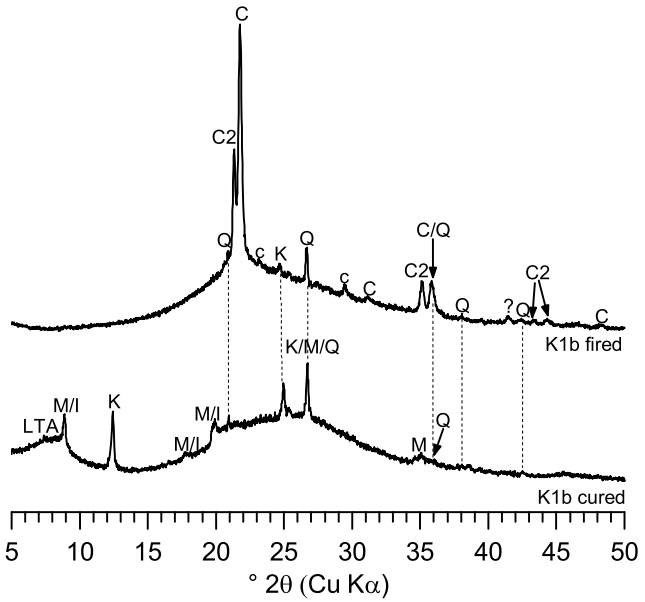

Fig. 3: Diffractograms of K1b and its fire residue (Q = quartz; C = cristobalite; C2 = intermediary carnegieite phase; c = calcite; M = muscovite; I = illite; K = kaolinite; LTA = zeolite Na-A).

After fire resistance testing of K1b, the zeolite Na-A had disappeared (Fig. 3). Again, cristobalite was the new major phase. In addition, significant amounts of an intermediary carnegieite phase (PDF # 00–049–002) formed, which parallels studies on other geopolymers. [25]. The reflections of most of the crystalline impurities from the metakaolin disappeared or diminished in the fire residue; however, a significant amount of quartz remained. Minor amounts of calcite were also observed, which formed most probably by carbonation of Ca-bearing impurities after the fire test and before the XRD investigations. The maximum of the amorphous hump shifted to a lower 2θ compared to the as-cured K1b; in the fire residue it is located at 21.6° 2θ, which is comparable to the diffractogram of C1 after fire testing.

In both, the C1 sample and the K1b sample, a small hump was present in the diffractograms at approx. 7–8° 2θ after curing, which disappeared after heating, the origin of which is not clear at present.

(2) Volume increase during curing and fire resistance testing

All coatings expanded during curing and again during fire resistance testing; the measured thicknesses are summarized in Table 4. The C1 coatings expanded by approx. 100 % during curing, while the K1b coatings expanded much less (between 15 % and 57 %). The expansion during curing occurred in a viscous state of the fresh pastes and parallels the behavior observed previously by Prud'homme *et al.* [37] and others [25,50] for geopolymers comprising microsilica. Prud'homme *et al.* deliberately used the microsilica as a foaming agent and explained the observed foaming with the reaction of metallic silicon, which is present as an impurity in many microsilicas (also in the present study; Fig. 1), with water in the highly alkaline environment and concomitant hydrogen release according to:

$$4H_2O + Si \rightarrow 2H_2 + Si(OH)_4 \qquad (1)$$

Table 4: Thickness of the coatings before and after curing, and of the fire residue after fire resistance testing.

	Before curing (mm)	After curing (mm)	Fire residue (mm)
C1	3	5.0 ± 1.4	19.4 ± 9.8
C1	5	9.9 ± 0.5	16.2 ± 1.9
C1	6	11.9 ± 1.4	21.7 ± 8.3
C1	7	15.0 ± 0.4	18.7 ± 0.6
C1	9	16.9 ± 0.5	19.8 ± 0.8
C1	12	28.8 ± 1.0	30.8 ± 1.7
K1b	2	2.3 ± 0.2	9.5 ± 4.8
K1b	3	4.7 ± 0.4	19.4 ± 4.4
K1b	5	7.0 ± 0.4	21.8 ± 4.2
K1b	6	8.1 ± 0.3	18.5 ± 4.0
K1b	7	10.0 ± 0.4	26.2 ± 6.0
K1b	9	14.1 ± 0.2	32.4 ± 5.7
K1b	12	17.9 ± 0.7	30.1 ± 4.3

Table 4 shows that expansion during fire resistance testing depended strongly on the original (uncured) thickness of the coating. The maximum expansion observed was for the coatings with the lowest thicknesses (original thickness ≤ 3 mm) which had an increase of thickness by approx. 300 %, compared to the thickness after curing. Expansion decreased considerably with increasing thickness of the coatings; this was particularly significant for the C1 coatings (7 % at 12 mm thickness), while the K1b coatings better retained their ability to expand at higher thicknesses (68 % at 12 mm thickness). The increase of thickness during the fire resistance testing was rather irregular for most coatings, particularly for low thicknesses, which resulted in the large uncertainties reported in Table 4. This is related to the fact that in many of the experiments large bubbles formed in the coatings, a phenomenon which is discussed further in Section IV (1).

Foaming and significant expansion on heating, as has been observed here, is atypical for geopolymers and has been reported previously only a few times [23,31,36,40,41]. In the following sections, results are presented that elucidate some aspects of the observed intumescent behavior.

(3) Thermogravimetric analyses and rheological properties

Fig. 4 shows the TGA results of C1, K1b and MK-ref (non-intumescing reference mix). Mass loss occurred at the highest rate in the temperature range approx. 50 – 200 °C; at temperatures above 200 °C, mass loss continued at a slightly slower rate and ceased at approx. 600 °C. This behavior is typical of geopolymers, as virtually all of the water in geopolymers is physically bound in their pores [42, 51 – 53] and therefore generally released at temperatures below 300 – 400 °C [19, 24, 28, 52]. The somewhat extended temperature range in which significant mass loss occurred in the present study is probably related to the heating rate of 10 K/min used during the TGA experiments.

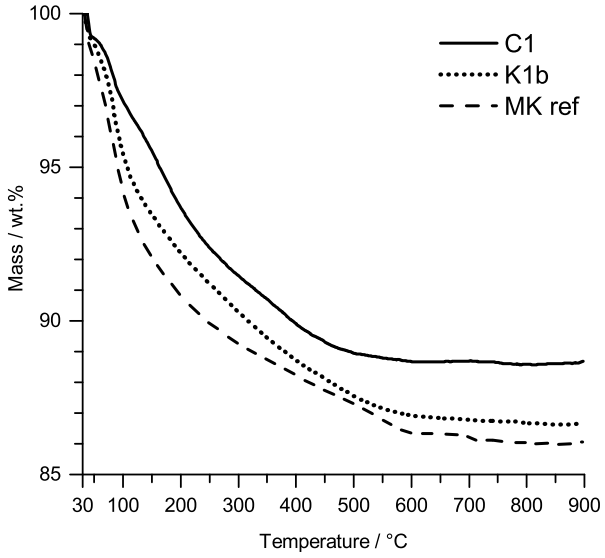

Fig. 4: TGA results of C1, K1b and MK-ref.

The recorded total mass losses (at 900 °C; *cf*. Fig. 4) differed between the formulations: MK-ref exhibited the highest mass loss of 13.9 wt% at 900 °C, while for C1 the lowest mass loss of 11.3 wt% was recorded. The relative order of the total mass losses parallels the relative order of the fraction of water in the starting mixes (Table 3).

The rheological properties of C1, K1b and MK-ref on heating up to 300 °C were studied by means of oscillatory rheometry; the results are shown in Fig. 5. For all samples, both the storage modulus, *G'*, and the loss modulus, *G"* exhibited a local minimum at approx. 100 – 150 °C. The values of MK-ref, in particular its loss modulus, exhibited large variations up to approx. 100 °C. Nevertheless, the measured values allow calculation at all temperatures of the loss factor (or loss tangent), tan δ, which is defined as [54]:

$$\tan \delta = G"/G' \qquad (2)$$

The loss factor is a measure of the relative contributions of viscous and elastic behavior to the response of the specimen, and as a first approximation one can suppose that a material behaves as a fluid (viscous behavior) if tan $\delta > 1$, and as a solid (elastic behavior) if tan $\delta < 1$ [55]. Thus, the most striking feature of Fig. 5b is that C1 and K1b exhibit fluid-like behavior over most of the temperature range 75 – 225 °C, while MK-ref behaves like an elastic solid up to 220 °C, and displays a loss factor only very slightly above unity in the range 220 – 275 °C.

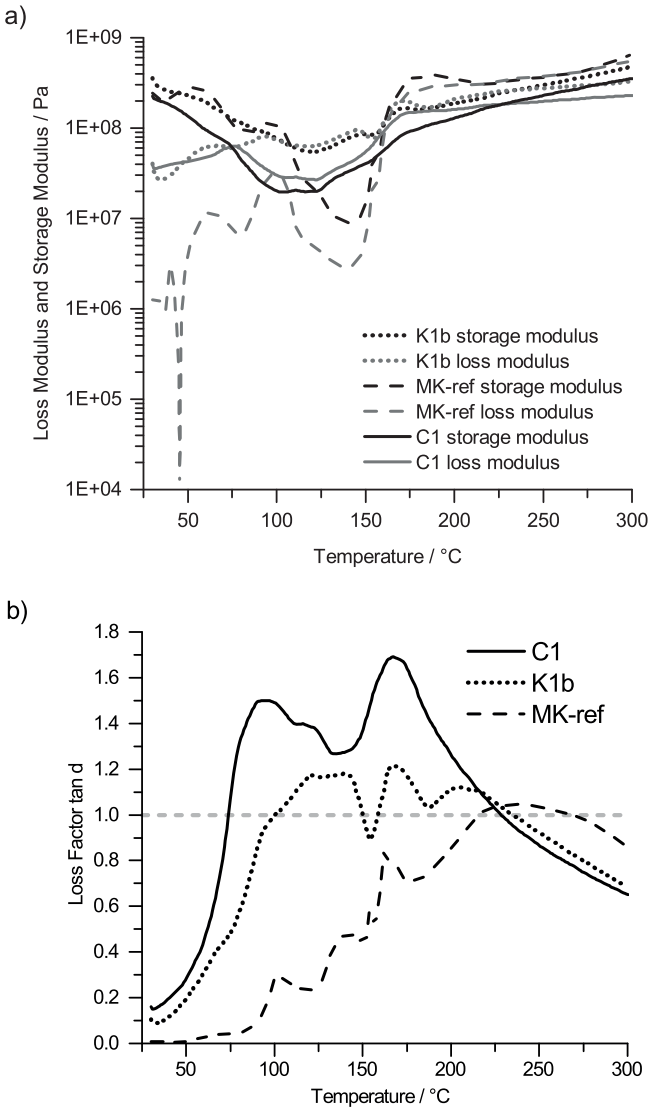

Fig. 5: a) Loss modulus and storage modulus *versus* temperature of C1, K1b and MK-ref; b) loss factor *versus* temperature of C1, K1b and MK-ref.

The temperature range in which C1 and K1b behave fluid-like, i.e. in which they are able to undergo viscous/plastic deformations, overlaps with the range of the highest mass loss rate in the TGA experiments (Fig. 4), while MK-ref is mainly solid-like over this temperature range. It is interpreted that this synchrony of fluid-like behavior and significant evaporation of water is a key aspect of the intumescent behavior of C1 and K1b. In cases where a geopolymer retains its elastic properties in the temperature range of rapid evaporation of water, as is the case for MK-ref and other conventional geopolymers, water vapor will simply escape through the pore system of the geopolymer, or – if its permeability is too low to release the vapor fast enough – will lead to the buildup of significant steam pressure and concomitant cracking [24, 28]. In addition to the release of water, the temperature increase may induce reaction of previously unreacted silica and associated hydrogen release due to metallic silicon impurities in the same temperature range, which would also contribute to the observed intumescent behavior.

An important factor contributing to the ability of certain aluminosilicate materials to show intumescence, as opposed to conventional geopolymers that are not intumescent, appears to be the amount of silica in the system: All intumescent formulations reported by Fletcher *et al.* [40] and Krivenko *et al.* [31] contained considerable amounts of microsilica, and the materials that exhibited intumescence in other studies [23,36,41] also had a comparatively high SiO_2/Al_2O_3 ratio. Provis *et al.* [41] suggested that this is linked to "excess molecular water and unreacted – and therefore poorly polymerized – silica" in the geopolymer, which remain when the starting mix has a high ratio of available SiO_2 over available Al_2O_3, i.e. a high effective SiO_2/Al_2O_3 molar ratio. This is also the case in the present study for K1b (addition of microsilica; Tables 2 and 3) as well as for C1 (only a small amount of the crystalline alumina had dissolved; see Section III (1)). However, the presence of microsilica does not necessarily lead to expansion during fire, as one-part geopolymers synthesized from microsilica and sodium aluminate do not exhibit intumescence [25]. The observed behavior of the intumescent formulations – and also their chemistry – resembles waterglass coatings (alkali silicate solutions/gels), which exhibit intumescent behavior that is based on the release of water at higher temperatures [56–58]; one may therefore regard these intumescent materials as a kind of geopolymer-bound 'stabilized waterglass'. However, it remains to be clarified how the presence of poorly reacted/polymerized silicate species in the material influences the transition to a viscous/plastic behavior in the temperature range of major water release.

(4) Microstructure before and after fire resistance testing

SEM micrographs after curing and after the fire tests of coating C1 and coating K1b are shown in Fig. 6 and Fig. 7, respectively. Both coatings exhibited extensive macroporosity in the form of spherical voids with diameters up to approx. 1 mm already after curing, in line with the observed foaming behavior and the proposed formation of hydrogen during curing (Section III (2)). The spherical macropores appeared to be more homogeneously distributed and to have a narrower size distribution in C1. At high magnification, both coatings exhibited a 'glassy' texture, typical of well-cured geopolymers. Additionally, in both samples remnants of the feedstocks are discernible (microsilica spheres with diameters of approx. 50–200 nm in C1; clay or metakaolin platelets and possibly also microsilica in K1b), in line with the XRD results (Section III (1)).

After the fire tests, the morphology of the macropores had changed, in particular for C1. The pores appeared to be larger and of an irregular shape, likely due to pore expansion and coalescence during heating. The micrograph at higher magnification of coating K1b (Fig. 7d) indicates that melting/viscous flow has taken place during heating in this sample.

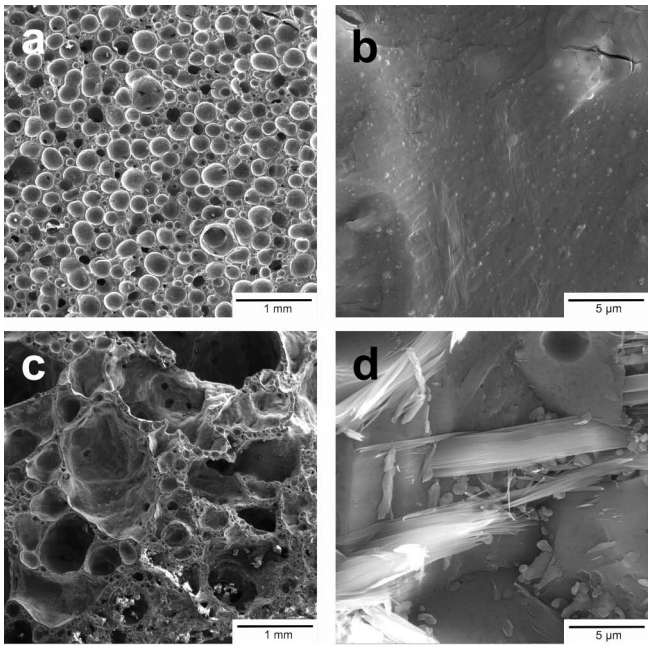

Fig. 6: SEM micrographs of the C1 coating a), b) after curing, and c), d) after the fire test.

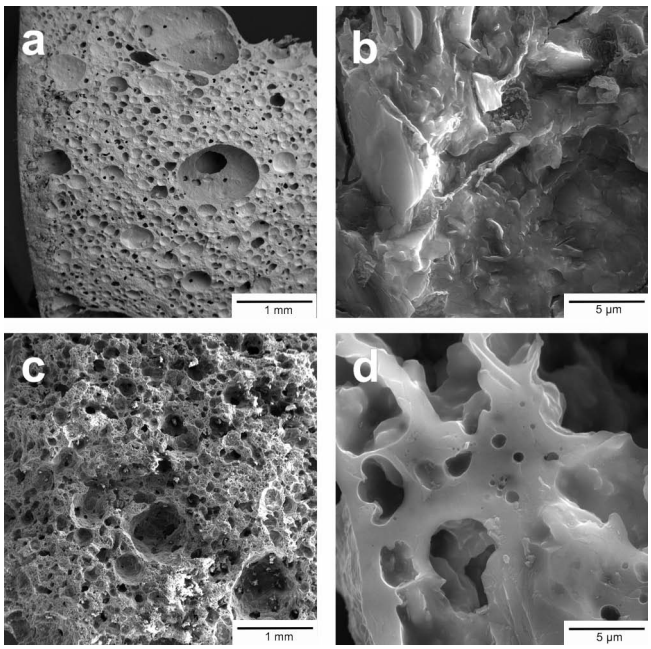

Fig. 7: SEM micrographs of the K1b coating a), b) after curing, and c), d) after the fire test.

IV. Temperature-Time Curves and Morphology of the Coatings after the Fire Resistance Tests

(1) Fire resistance of the coatings without additives

Fig. 8 shows the temperature-time curves of the C1 and K1b coatings. In the temperature-time curves of all coatings a plateau at approx. 100 °C was present after the initial temperature increase. At this temperature, much of the water in the coatings evaporates, and, according to the findings in Section III, intumescence of the coatings begins. The time period of the plateau increased with increasing thickness of the coatings, which is related to the amount of water in the samples. After the plateau has ended, the temperature at the back side of the coated steel plates increased at a nearly constant rate for 2 mm and

3 mm coating thickness, or increasing rate for the other coatings. The backside of the uncoated steel plated reached 500 °C (at which structural steel loses approx. 50 % of its yield stress at room temperature) in less than nine minutes, whereas the plates with just a few millimeters of coating took more than 20 minutes to reach the same temperature. Thicker coatings provided better protection; coating C1 with a layer thickness of 12 mm was able to protect the back side of the steel plate from a temperature increase to ≥ 500 °C for more than 30 min.

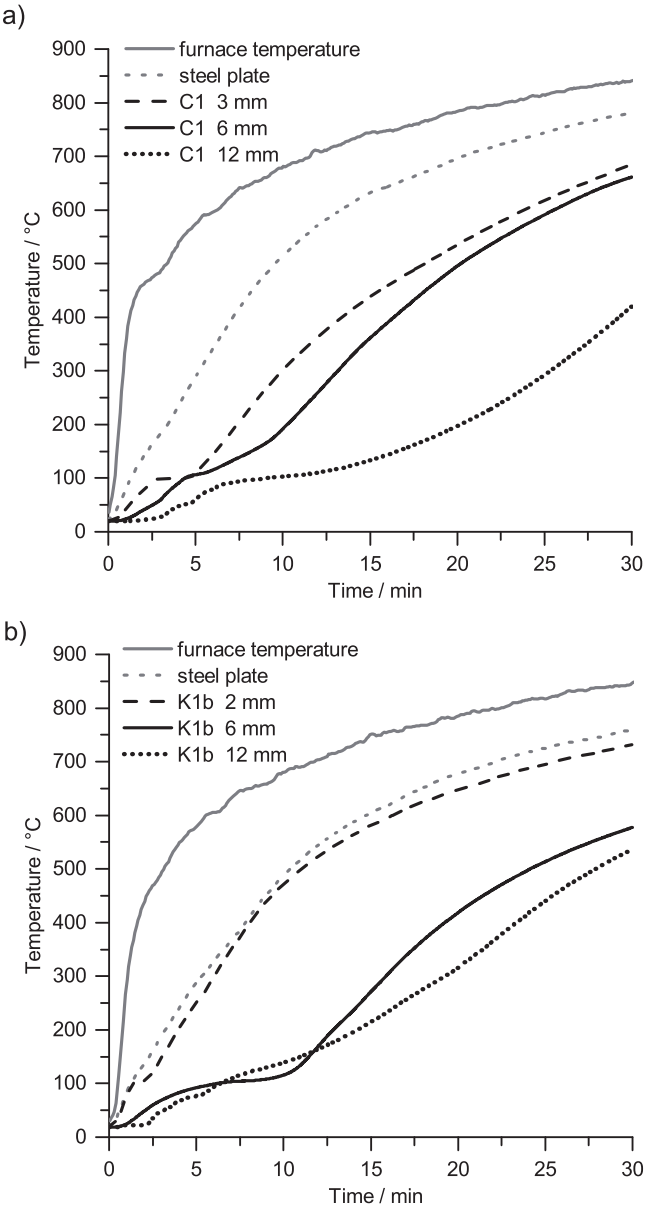

Fig. 8: Temperature-time curves for a) C1 coatings and b) K1b coatings with layer thicknesses of 2 or 3, 6 and 12 mm. The temperature-time curve for an uncoated steel plate and the temperature within the furnace are included for comparison.

As expected, thicker coatings exhibited better fire resistance. From Fig. 8 and Table 4, it is also clear, however, that there is no linear correlation between the coating thickness before or after curing and the performance of the coatings. For example, C1 coatings with 3-mm and 6-mm thickness demonstrated similar performance, while the 12-mm coating performed much better. (Furthermore, the protection effect ceased for coatings that detached from the steel plate during the fire test, i.e. the 2-mm K1b coating.) On the other hand, the fire resistance correlates well with the thickness of the fire residues, particularly for K1b samples. In Fig. 9, the time to reach 500 °C versus coating thickness *after* the fire tests is plotted. Fig. 9 contains additional samples not shown in Fig. 8. The coatings showed significant variations in the thickness of their fire residues, but an approximately linear correlation was clearly observed with the fire resistance, here defined as the time for the back side of the coated steel plate to reach 500 °C. This result is reasonable, as (1) a larger layer thickness corresponds to a larger original thickness and, therefore, to a higher water content per unit area of the coating, which will extend the duration of the plateau at approx. 100 °C in the temperature-time curves, and (2) a larger insulating fire residue thickness after intumescence, which happens most likely in the temperature range of approx. 75 – 225 °C (Section III (3)), leads to a decreased heat transfer through the coating to the steel plate at higher temperatures.

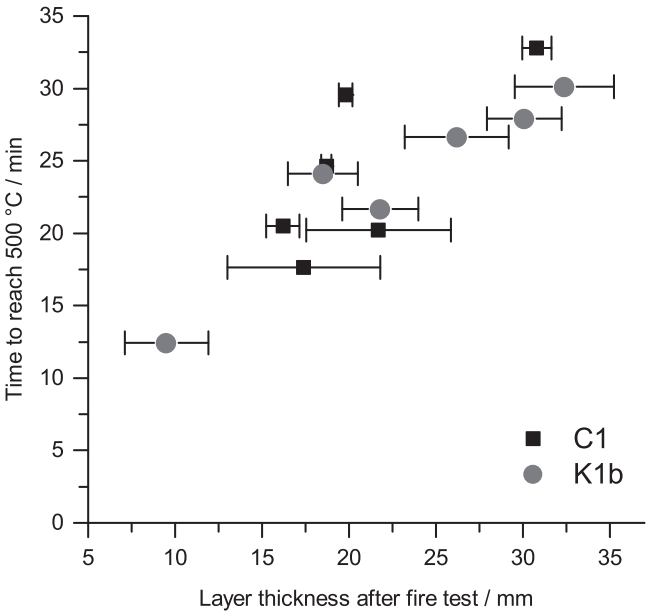

Fig. 9: Time to reach 500 °C on the back side of the coated steel plate during fire test *versus* layer thickness of the fire residue for C1 and K1b specimens.

Cross-sections of the fire residues of C1 and K1b coatings are shown in Figs. 10 and 11, respectively. The coatings with a low thickness (≤ 3 mm) expanded mainly as a result of the formation of one large bubble in the center of the specimen or four larger bubbles in the corners of the specimen. These larger pores seem to integrate all the evolved gases during fire resistance testing below a relatively dense yet porous shell. In contrast, the coatings with a higher thickness (6 mm or 12 mm) exhibited more uniform multicellular expansion and thus the formation of smaller pores, leading to a more homogeneous, foam-like structure. This formation of a multicellular foam structure is assumed to be advantageous, as it is expected to result in superior mechanical stability and thermal insulation during and after a fire.

For both materials, C1 and K1b, the behavior of coatings with 6-mm thickness varied between samples. While some of them showed expansion mainly *via* foam formation (Fig. 10b), others exhibited formation of a single large

bubble (not shown; similar to the coatings with 2- or 3-mm thickness) although they were prepared under the same conditions. Thus, it is thought that a coating thickness of 6 mm must approximate the minimum thickness to ensure a uniform, foam-like expansion. All the coatings were observed to have delaminated from the steel plates after fire testing. However, visual observation and the test data indicated that the delamination only occurred upon cooling and not during the high-temperature exposure, with the exception of the K1b 2-mm sample which was observed to detach during the test (*cf*. Fig. 8b).

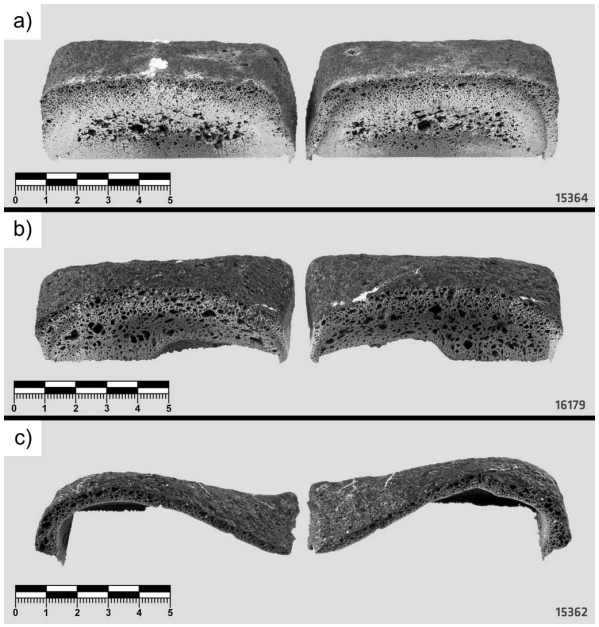

Fig. 10: C1 coatings with layer thicknesses of a) 12 mm, b) 6 mm, c) 3 mm, after the fire tests. (Scale bars in cm. The white precipitates on the cut surfaces formed after cutting, i.e. after contact with water and air; probably sodium carbonates.)

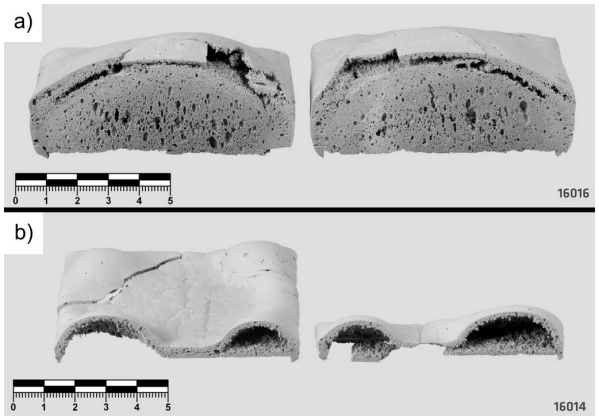

Fig. 11: K1b coatings with layer thicknesses of a) 12 mm, b) 2 mm, after the fire tests. (Scale bars in cm.)

(2) Influence of additives

Aluminum hydroxide ($Al(OH)_3$) and magnesium hydroxide ($Mg(OH)_2$) are very common flame retardants [59,60], but also interesting ingredients for multicomponent approaches to tackle fire resistance, as they act as 'heat sinks' *via* endothermal decomposition at elevated temperatures accompanied by the release of water vapor. Decomposition temperatures of the two compounds depend on heating conditions, particle size, present polymorphs, impurities, etc., but are approximately in the range 150–350 °C and 350–450 °C for aluminum hydroxide and magnesium hydroxide, respectively [59,60].

Coatings were prepared with 10 wt% or 20 wt% of either aluminum hydroxide or magnesium hydroxide; higher amounts of these additives led to pastes with unsatisfactory workability. All coatings were produced with an original thickness of 6 mm. The temperature-time curves of the coatings are shown in Fig. 12. For the C1 coatings the addition of aluminum hydroxide and of magnesium hydroxide improved the insulating properties of the coating from around 21 minutes to reach 500 °C to 22–27 minutes, while for the K1b coatings the additives led to lower performance. A distinct plateau caused by the decomposition of the hydroxides was not observed in the fire tests, although for C1 with 20 wt% $Al(OH)_3$ a slight decrease in the slope of the temperature-time curve around 250 °C did occur. The endothermic decomposition and water release of the metal hydroxides occurred more continuously during the first minutes of the fire test, most probably caused by the temperature gradient of the coating during fire resistance testing.

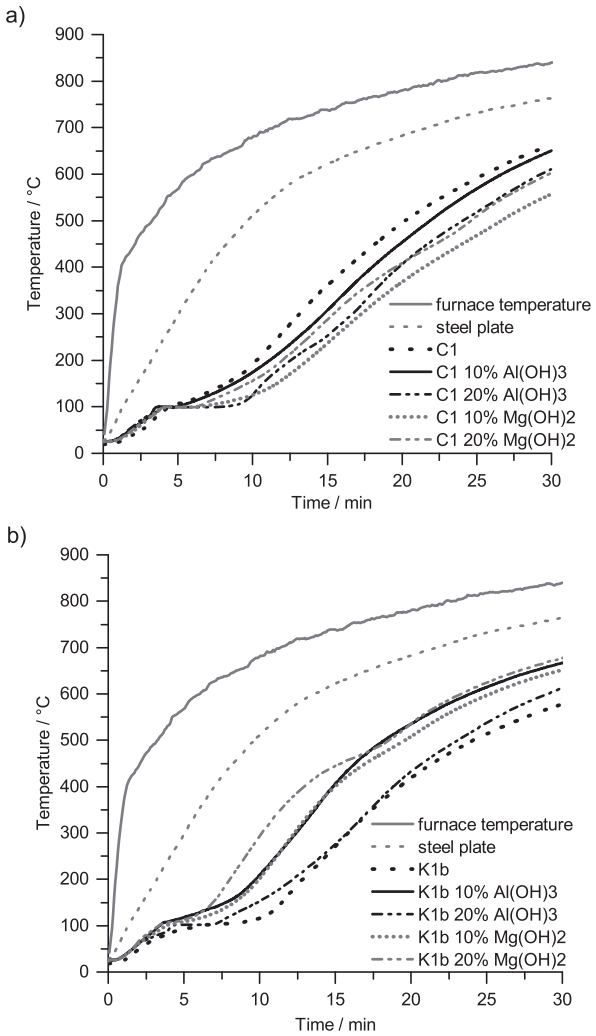

Fig. 12: Temperature-time curves for a) C1 coatings and b) K1b coatings with 10 wt% or 20 wt% $Al(OH)_3$, or 10 wt% or 20 wt% $Mg(OH)_2$ with layer thickness of 6 mm. The temperature-time curves for the C1 coating and the K1b coating with layer thickness of 6 mm and for an uncoated steel plate and the temperature within the furnace are included for comparison.

Different boron compounds are commonly used to improve the fire performance owing to the formation of glassy surface coatings [61, 62]; their properties and applications have been reviewed by Shen *et al.* [63]. Boron trioxide (B_2O_3) is soluble in water, giving boric acid ($B(OH)_3$). Anhydrous sodium tetraborate ($Na_2B_4O_7$) was effectively applied as a glass former and for 'ceramification' during polymer combustion [63]. Its dissolution rate in water can be expected to depend on particle size, degree of crystallinity, etc.; the stable solid in a saturated aqueous sodium tetraborate solution below approx. 60 °C is sodium tetraborate decahydrate ($Na_2B_4O_7{\cdot}10H_2O$; borax), not the anhydrous compound. Sodium tetraborate was used by Krivenko *et al.* [31] as an additive for fire-protective aluminosilicate coatings; in their study, addition of sodium tetraborate accelerated hardening of the coating but did not lead to increased intumescence.

Temperature-time curves of C1 coatings with the addition of boron trioxide, sodium tetraborate or both are shown in Fig. 13. The addition of 10 wt% boron trioxide decreased the performance of the coating compared to the neat C1 coating, while 10 wt% sodium tetraborate significantly improved the performance of the coating, shifting the time to reach 500 °C from 21 to 30 minutes. Impressively, the addition of 10 wt% sodium tetraborate to the 6-mm-thick C1 coating yielded an equivalent fire resistance to the original C1 coating with double the thickness (the 12-mm C1 sample yielded a 30-minute fire resistance). In the coating with 5 wt% of each of these additives their opposing effects were counteracted by each other, resulting in a time-temperature curve very similar to that of the C1 coating.

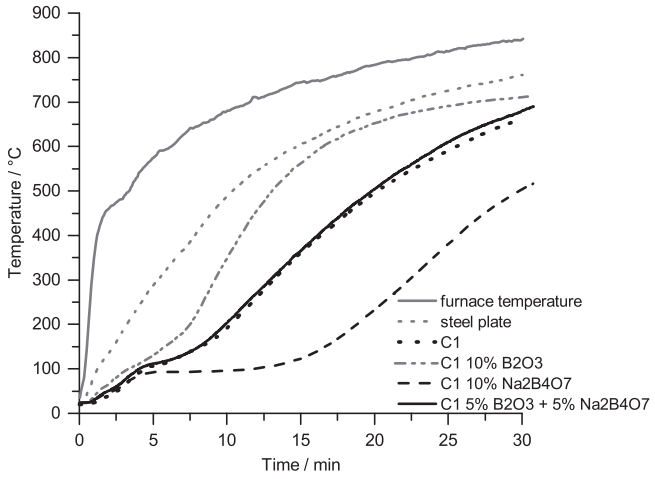

Fig. 13: Temperature-time curves for C1 coatings with 10 wt% B_2O_3, 10 wt% $Na_2B_4O_7$, or 5 wt% B_2O_3 + 5 wt% $Na_2B_4O_7$ with layer thickness of 6 mm. The temperature-time curves for the C1 coating with original layer thickness of 6 mm and for an uncoated steel plate and the temperature within the furnace are included for comparison.

The C1 coating with 10 wt% sodium tetraborate exhibited a distinct plateau at approx. 95 – 100 °C, which extended over a much longer time period than for the C1 coating. This extended plateau is largely responsible for the much-improved performance. It is likely that the sodium tetraborate had at least partly dissolved in the activating solution of the fresh coating, leading to precipitation of sodium borate hydrates on curing and storage at 23 °C/50 % RH prior to the fire test. These compounds would then have given off water at the temperature of the plateau, keeping the temperature approximately constant by evaporation until depleted.

In supplementary experiments, 1 g of the sodium tetraborate was suspended in 500 ml of 12 M NaOH solution (equivalent to 27.1 wt% Na_2O, i.e. very similar to the NaOH solution employed for activation of mix C1) and the suspension was allowed to stand at room temperature for 48 h. Subsequently, the resulting suspension was filtered, the filter residue rinsed with 2-propanol and vacuum dried (p = 40 mbar; $T \approx 25$ °C) overnight. XRD of the filtration residue (results not displayed) showed it to be composed almost entirely of sodium metaborate dihydrate ($NaBO_2{\cdot}2H_2O$ or $NaB(OH)_4$); this compound is known to dehydrate above approx. 90 °C [64]. These results are in good agreement with the described hypothesis about the molecular mechanisms of sodium tetraborate in the coating.

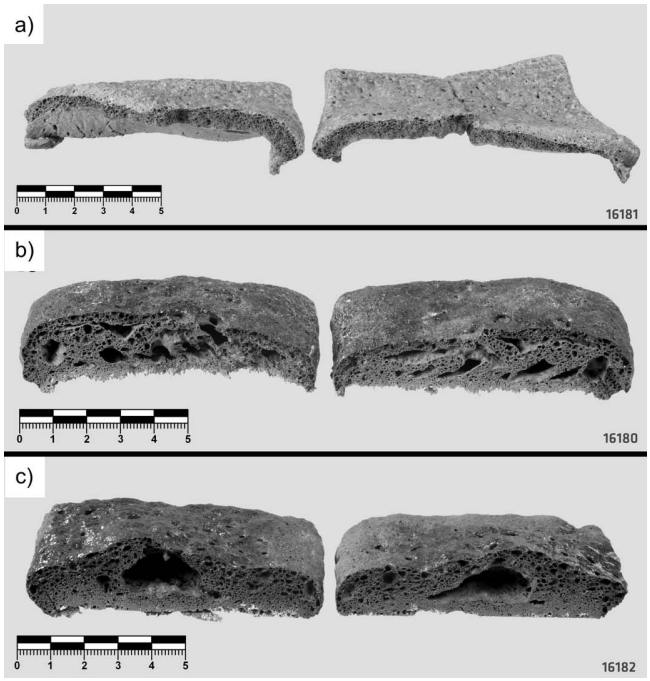

Fig. 14: C1 coatings with a) 10 wt% B_2O_3, b) 10 wt% $Na_2B_4O_7$, c) 5 wt% B_2O_3 + 5 wt% $Na_2B_4O_7$ with original (uncured) layer thickness of 6 mm, after the fire tests. (Scale bars in cm.)

Cross-sections obtained by cutting the fire residues of the C1 coatings with boron compounds after the fire tests are shown in Fig. 14. The C1 coating with 10 wt% boron trioxide revealed the formation of a large bubble, i.e. undesirable behavior. In contrast, the C1 coating with 10 wt% sodium tetraborate displayed a spongy microstructure, revealing some larger and coalesced pores/voids, but still retaining a coherent structure that extends to the substrate. The behavior of the C1 coating with 5 wt% boron trioxide + 5 wt% sodium tetraborate appeared to be intermediate: the coating was still in contact with the substrate, although a comparatively large bubble formed inside the coating. Fig. 14 also shows that the surfaces of all coatings

with the addition of boron compounds appear to be glossy, indicating that the additives were effective as glass-forming agents.

V. Conclusions

Intumescent aluminosilicate coatings, based either on microsilica and alumina (C1) or on metakaolin and microsilica (K1b), were investigated for use as fire-resistant intumescent coatings. During curing at 40 °C foaming of the coatings occurred, which was attributed to the formation of hydrogen by reaction of silicon impurities in the microsilica with the alkaline activator solution. During fire resistance testing the coatings expanded further, i.e. they exhibited intumescent behavior. The ability of the materials to expand during heating without cracking was explained by rheological testing, which revealed that the samples behaved in a viscous manner during the dehydrating-water-driven expansion event (between 75 and 225 °C). This was in contrast to the behavior of a 'standard' metakaolin-based geopolymer, which dehydrated in the same temperature range, yet rheologically behaved as a solid throughout the heating process.

The degree of intumescence depended on the mix-design and the coating thickness. Generally, reduced intumescence was observed with thicker coatings; this was more pronounced for the C1 coatings, while the K1b coatings better retained their ability to expand at higher thickness. Fire testing showed that a minimum coating thickness of approx. 6 mm was required to achieve satisfactory insulating behavior, with 12-mm thickness protecting a steel plate for > 30 min. The coatings exhibited characteristics of ceramic or glass-ceramic foams after fire resistance testing. This is thought to be an advantage under fire conditions where higher temperatures are reached or where mechanical stability of the coating is required.

Several additives were tested to improve the fire resistance of the coatings. The best results were obtained with the addition of 10 wt% anhydrous sodium tetraborate, leading to a performance of the 6-mm-thick C1 coating with addition being very similar to that of the neat C1 coating with 12 mm thickness. This was mainly related to an extended temperature plateau at approx. 95 – 100 °C, attributed to the formation of hydrous sodium metaborate during curing and subsequent storage, and its dehydration during heating.

In summary, intumescent aluminosilicate (geopolymer-bound) composites were reported to show fire-resistant properties and to be promising materials for fire-protective coatings. These results warrant further studies on their performance. Future optimization may even open the route for developing thin intumescent coatings based on geopolymers.

Acknowledgments

The authors thank C. Huth for technical assistance with the rheological measurements, and M. Lindemann for the chemical analyses (ICP-OES) and assistance with the wet chemical experiments. The instrument used for the SEM analysis is supported by the Australian Science and Industry Endowment Fund.

References

1 Vandersall, H.: Intumescent coating systems, their development and chemistry, *J. Fire Flammability*, **2**, 97 – 140, (1971).

2 Bartholmai, M., Schriever, R., Schartel, B.: Influence of external heat flux and coating thickness on thermal insulation properties of two different intumescent coatings using cone calorimeter and numerical analysis, *Fire Mater.*, **27**, 151 – 162, (2003).

3 Duquesne, S., Magnet, S., Jama, C., Delobel, R.: Intumescent paints: Fire protective coatings for metallic substrates. *Surf. Coat. Technol.*, **180**, 302 – 307, (2004).

4 Jimenez, M., Duquesne, S., Bourbigot, S.: Intumescent fire protective coating: Toward a better understanding of their mechanism of action, *Thermochim. Acta*, **449**, 16 – 26, (2006).

5 Gu, J.W., Zhang, G.C., Dong, S.L., Zhang, Q.Y., Kong, J.: Study on preparation and fire-retardant mechanism analysis of intumescent flame-retardant coatings, *Surf. Coat. Technol.*, **201**, 7835 – 7841, (2007).

6 Bartholmai, M., Schartel, B.: Assessing the performance of intumescent coatings using bench-scaled cone calorimeter and finite difference simulations, *Fire Mater.*, **31**, 187 – 205, (2007).

7 Duquesne, S., Bachelet, P., Bellayer, S., Bourbigot, S., Mertens, W.: Influence of inorganic fillers on the fire protection of intumescent coatings. *J. Fire Sci.*, **31**, 258 – 275, (2013).

8 Weil, E.D.: Fire-protective and flame-retardant coatings – a state-of-the-art review, *J. Fire Sci.*, **29**, 259 – 296, (2011).

9 Alongi, J., Han, Z., Bourbigot, S.: Intumescence: tradition versus novelty. A comprehensive review, *Prog. Polym. Sci.*, **51**, 28 – 73, (2015).

10 Mariappan, T.: Recent developments of intumescent fire protection coatings for structural steel: A review, *J. Fire Sci.*, **34**, 120 – 163, (2016).

11 Gardelle, B., Duquesne, S., Vandereecken, P., Bellayer, S., Bourbigot, S.: Resistance to fire of intumescent silicone based coating: The role of organoclay, *Prog. Org. Coat.*, **76**, 1633 – 1641, (2013).

12 Gardelle, B., Duquesne, S., Vandereecken, P., Bourbigot, S.: Characterization of the carbonization process of expandable graphite/silicone formulations in a simulated fire, *Polym. Degrad. Stab.*, **98**, 1052 – 1063, (2013).

13 Gardelle, B., Duquesne, S., Vandereecken, P., Bourbigot, S.: Resistance to fire of silicone-based coatings: fire protection of steel against cellulosic fire, *J. Fire Sci.*, **32**, 374 – 387, (2014).

14 Kruse, D., Simon, S., Menke, K., Friebel, S., Gettwert, V.: Composition for a fire-protection agent for materials and fire-protection method. European Patent EP 1 678 268, (2004).

15 Hörold, A., Schartel, B., Trappe, V., Gettwert, V., Korzen M.: Protecting the structural integrity of composites in fire: intumescent coatings in the intermediate scale, *J. Reinf. Plast. Compos.*, **34**, 2029 – 2044, (2015).

16 Krüger, S., Gluth, G.J.G., Watolla, M.-B., Morys, M., Hässler, D., Schartel, B.: New ways: reactive fire protection coatings for extreme conditions, (in German), *Bautechnik*, **93**, 531 – 542, (2016).

17 Duxson, P., Fernández-Jiménez, A., Provis, J.L., Lukey, G.C., Palomo, A., van Deventer, J.S.J.: Geopolymer technology: The current state of the art, *J. Mater. Sci.*, **42**, 2917 – 2933, (2007).

18 Provis, J.L., Bernal, S.A.: Geopolymers and related alkali-activated materials, *Annu. Rev. Mater. Res.*, **44**, 299 – 327, (2014).

19 Barbosa, V.F.F., MacKenzie, K.J.D.: Thermal behaviour of inorganic geopolymers and composites derived from sodium polysialate, *Mater. Res. Bull.*, **38**, 319 – 331, (2003).

20 Comrie, D.C., Kriven, W.M.: Composite cold ceramic geopolymer in a refractory application, *Ceram. Trans.*, **153**, 211 – 225, (2003).

21 Fernández-Jiménez, A., Palomo, A., Pastor, J.Y., Martín, A.: New cementitious materials based on alkali-activated fly ash:

performance at high temperatures, *J. Am. Ceram. Soc.*, **91**, 3308 – 3314, (2008).

22 Bell, J.L., Driemeyer, P.E., Kriven, W.M.: Formation of ceramics from metakaolin-based geopolymers. Part II: K-based geopolymer, *J. Am. Ceram. Soc.*, **92**, 607 – 615, (2009).

23 Rickard, W.D.A., Temuujin, J., van Riessen, A.: Thermal analysis of geopolymer pastes synthesised from five fly ashes of variable composition, *J. Non-Cryst. Solids*, **358**, 1830 – 1839, (2012).

24 Rickard, W.D.A., Kealley, C.S., van Riessen, A.: Thermally induced microstructural changes in fly ash geopolymers: Experimental results and proposed model, *J. Am. Ceram. Soc.*, **98**, 929 – 939, (2015).

25 Sturm, P., Gluth, G.J.G., Simon, S., Brouwers, H.J.H., Kühne, H.-C.: The effect of heat treatment on the mechanical and structural properties of one-part geopolymer-zeolite composites, *Thermochim. Acta*, **635**, 41 – 58, (2016).

26 Bell, J., Gordon, M., Kriven, W.: Use of geopolymeric cements as a refractory adhesive for metal and ceramic joins, *Ceram. Eng. Sci. Proc.*, **26**, [3], 407 – 413, (2005).

27 Zhao, R., Sanjayan, J.G.: Geopolymer and portland cement concretes in simulated fire, *Mag. Concr. Res.*, **63**, 163 – 173, (2011).

28 Rickard, W.D.A., Gluth, G.J.G., Pistol, K.: In-situ thermo-mechanical testing of fly ash geopolymer concretes made with quartz and expanded clay aggregates, *Cem. Concr. Res.*, **80**, 33 – 43, (2016).

29 Gluth, G.J.G., Rickard, W.D.A., Werner, S., Pirskawetz, S.: Acoustic emission and microstructural changes in fly ash geopolymer concretes exposed to simulated fire, *Mater. Struct.*, **49**, 5243 – 5254, (2016).

30 Herr, R.: Geopolymers – a new mineral construction materials generation for the fire protection of civil engineering structures, (in German), IEMB Info 2004/7. Institut für Erhaltung und Modernisierung von Bauwerken, Berlin, 2004.

31 Krivenko, P.V., Pushkavera, Y.K., Sukhanevich, M.V., Guziy, S.G.: Fireproof coatings on the basis of alkaline aluminum silicate systems, *Ceram. Eng. Sci. Proc.*, **29**, [10], 129 – 142, (2009).

32 Temuujin, J., Minjigmaa, A., Rickard, W., Lee, M., Williams, I., van Riessen, A.: Fly ash based geopolymer thin coatings on metal substrates and its thermal evaluation, *J. Hazard. Mater.*, **180**, 748 – 752, (2010).

33 Rickard, W.D.A., Vickers, L., van Riessen, A.: Performance of fibre reinforced, low density metakaolin geopolymers under simulated fire conditions, *Appl. Clay Sci.*, **73**, 71 – 77, (2013).

34 Rickard, W.D.A., van Riessen, A.: Performance of solid and cellular structured fly ash geopolymers exposed to a simulated fire, *Cem. Concr. Compos.*, **48**, 75 – 82, (2014).

35 Sakkas, K., Nomikos, P., Sofianos, A., Panias, D.: Sodium-based fire resistant geopolymer for passive fire protection, *Fire Mater.*, **39**, 259 – 270, (2015).

36 Lyon, R.E., Balaguru, P.N., Foden, A., Sorathia, U., Davidovits, J., Davidovics, M.: Fire-resistant aluminosilicate composites, *Fire Mater.*, **21**, 67 – 73, (1997).

37 Prud'homme, E., Michaud, P., Joussein, E., Peyratout, C., Smith, A., Arrii-Clacens, S., Clacens, J.M., Rossignol, S.: Silica fume as porogent agent in geo-materials at low temperature, *J. Eur. Ceram. Soc.*, **30**, 1641 – 1648, (2010).

38 Masi, G., Rickard, W.D.A., Vickers, L., Bignozzi, M.C., van Riessen, A.: A comparison between different foaming methods for the synthesis of light weight geopolymers, *Ceram. Int.*, **40**, 13891 – 13902, (2014).

39 Hlaváček, P., Šmilauer, V., Škvara, F., Kopecký, L., Šulc, R.: Inorganic foams made from alkali-activated fly ash: Mechanical, chemical and physical properties, *J. Eur. Ceram. Soc.*, **35**, 703 – 709, (2015).

40 Fletcher, R.A., MacKenzie, K.J.D., Nicholson, C.L., Shimada, S.: The composition range of aluminosilicate geopolymers, *J. Eur. Ceram. Soc.*, **25**, 1471 – 1477, (2005).

41 Provis, J.L., Harrex, R.M., Bernal, S.A., Duxson, P., van Deventer, J.S.J.: Dilatometry of geopolymers as a means of selecting desirable fly ash sources, *J. Non-Cryst. Solids*, **358**, 1930 – 1937, (2012).

42 Rahier, H., van Mele, B., Biesemanns, M., Wastiels, J., Wu, X.: Low-temperature synthesized aluminosilicate glasses. Part I. Low-temperature reaction stoichiometry and structure of a model compound, *J. Mater. Sci.*, **31**, 71 – 79, (1996).

43 Steveson, M., Sagoe-Crentsil, K.: Relationships between composition, structure and strength of inorganic polymers. Part I — metakaolin-derived inorganic polymers, *J. Mater. Sci.*, **40**, 2023 – 2036, (2005).

44 Duxson, P., Provis, J.L., Lukey, G.C., Mallicoat, S.W., Kriven, W.M., van Deventer, J.S.J.: Understanding the relationship between geopolymer composition, microstructure and mechanical properties, *Colloids Surf. A*, **269**, 47 – 58, (2005).

45 Duxson, P., Provis, J.L., Lukey, G.C., Separovic, F., van Deventer, J.S.J.: ^{29}Si NMR study of structural ordering in aluminosilicate geopolymer gels, *Langmuir*, **21**, 3028 – 3036, (2005).

46 Provis, J.L., Lukey, G.C., van Deventer, J.S.J.: Do geopolymers actually contain nanocrystalline zeolites? A reexamination of existing results, *Chem. Mater.*, **17**, 3075 – 3085, (2005).

47 Salmang, H., Scholze, H., Telle, R.: Ceramics, in German, 7th edition. Springer, Berlin, 2007.

48 Cole, S.S.: The conversion of quartz into cristobalite below 1000 °C, and some properties of the cristobalite formed, *J. Am. Ceram. Soc.*, **18**, 149 – 154, (1935).

49 Beneke, K., Lagaly, G.: A hydrated potassium layer silicate and its crystalline silicic acid, *Am. Mineral.*, **74**, 224 – 229, (1989).

50 Krivenko, P.V., Kovalchuk, G.Y.: Fly-ash based zeolite cements. In: Innovations and Developments in Concrete Materials and Construction. Thomas Telford, London, 2002; 123 – 132.

51 Perera, D.S., Vance, E.R., Finnie, K.S., Blackford, M.G., Hanna, J.V., Cassidy, D.J., Nicholson, C.L.: Disposition of water in metakaolinite based geopolymers, *Ceram. Trans.*, **175**, 225 – 236, (2006).

52 Duxson, P., Lukey, G.C., van Deventer, J.S.J.: Physical evolution of Na-geopolymer derived from metakaolin up to 1000 °C, *J. Mater. Sci.*, **42**, 3044 – 3054, (2007).

53 Greiser, S., Sturm, P., Gluth, G.J.G., Hunger, M., Jäger, C.: Differentiation of the solid-state NMR signals of gel, zeolite phases and water species in geopolymer-zeolite composites, *Ceram. Int.*, **43**, 2202 – 2208, (2017).

54 Macosko, C.W.: Rheology: Principles, measurements, and applications. Wiley-VCH, New York, 1994.

55 Poulesquen, A., Frizon, F., Lambertin, D.: Rheological behavior of alkali-activated metakaolin during geopolymerization, *J. Non-Cryst. Solids*, **357**, 3565 – 3571, (2011).

56 Bulewicz, E.M., Pelc, A., Kozlowski, R., Miciukiewicz, A.: Intumescent silicate-based materials: mechanism of swelling in contact with fire, *Fire Mater.*, **9**, 171 – 175, (1985).

57 Langille, K.B., Nguyen, D., Bernt, J.O., Veinot, D.E., Murthy, M.K.: Mechanism of dehydration and intumescence of soluble silicates. Part I: effect of silica to metal oxide molar ratio, *J. Mater. Sci.*, **26**, 695 – 703, (1991).

58 Langille, K.B., Nguyen, D., Bernt, J.O., Veinot, D.E., Murthy, M.K.: Mechanism of dehydration and intumescence of soluble silicates. Part II: effect of the cation, *J. Mater. Sci.*, **26**, 704 – 710, (1991).

59 Horn, W.E.: Inorganic hydroxides and hydroxycarbonates: Their function and use as flame retardants. In: Fire Retardancy of Polymeric Materials. Marcel Dekker, New York, 2000; pp. 285 – 352.

[60] Hornsby, P.: Fire-retardant fillers. In: Fire Retardancy of Polymeric Materials. 2nd edition. CRC Press, Boca Raton, 2010; pp. 163 – 185.

[61] Pawlowski, K.H., Schartel, B., Fichera, M.A., Jäger, C.: Flame retardancy mechanisms of bisphenol A bis(diphenyl phosphate) in combination with zinc borate in bisphenol A polycarbonate/acrylonitrile-butadiene-styrene blends, *Thermochim. Acta*, **498**, 92 – 99, (2010).

[62] Wawrzyn, E., Schartel, B., Karrasch, A., Jäger, C.: Flame-retarded bisphenol A polycarbonate/silicon rubber/bisphenol A bis(diphenyl phosphate): Adding inorganic additives, *Polym. Degrad. Stab.*, **106**, 74 – 87, (2014).

[63] Shen, K.K., Kochesfahani, S.H., Jouffret, F.: Boron-based flame retardants and flame retardancy. In: Fire Retardancy of Polymeric Materials. 2nd edition. CRC Press, Boca Raton, 2010; pp. 207 – 238.

[64] Beaird, A.M., Li, P., Marsh, H.S., Al-Saidi, W.A., Johnson, J.K., Matthews, M.A., Williams, C.T.: Thermal dehydration and vibrational spectra of hydrated sodium metaborates, *Ind. Eng. Chem. Res.*, **50**, 7746 – 7752, (2011).